Effect of streamwise surface undulations on the nonlinear stability of crossflow instabilities

Westerbeek, S.; Kotsonis, M.

Publication date
2022

Document Version
Final published version

Citation (APA)
Westerbeek, S., & Kotsonis, M. (2022). *Effect of streamwise surface undulations on the nonlinear stability of crossflow instabilities*. Paper presented at 12th International Symposium on Turbulence and Shear Flow Phenomena, TSFP 2022, Osaka, Virtual, Japan.

Important note
To cite this publication, please use the final published version (if applicable).
Please check the document version above.

12th International Symposium on Turbulence and Shear Flow Phenomena (TSFP12)
Osaka, Japan (Online), July 19-22, 2022

EFFECT OF STREAMWISE SURFACE UNDULATIONS ON THE NONLINEAR STABILITY OF CROSSFLOW INSTABILITIES

S. Westerbeek
Faculty of Aerospace Engineering
TU Delft
Leeghwaterstraat 42, 2628 CA Delft
S.H.J.Westerbeek@tudelft.nl

M. Kotsonis
Faculty of Aerospace Engineering
TU Delft
Leeghwaterstraat 42, 2628 CA Delft
M.Kotsonis@tudelft.nl

ABSTRACT

The nonlinear stability of three-dimensional boundary layers over various undulated surfaces was calculated using the generalized Nonlinear Parabolized Stability Equations (NPSE). The results are compared with a flat plate configuration to assess the effect of the undulation shape on the stability of the boundary layer. It was found that the effect of surface undulations is significant and should not be ignored when performing stability analysis. All undulation shapes considered in this work showed a destabilization of the primary mode and the associated harmonics. The stability of the boundary layer was directly affected by the amplitude of the undulations, while their respective shape did not meaningfully affect the evolution of the crossflow instabilities within the parameter range considered in this work.

Introduction

The laminar-to-turbulent transition of boundary layers directly affects the skin friction drag experienced by an aircraft wing resulting in increased fuel costs and associated emissions. At the same time, the manufacturing of wings is subject to limitations resulting in necessary junctions (gaps and steps) and bolts on the wing surface. Furthermore, plate rolling techniques and operational loads affect the surface smoothness of the wing plate itself, by inherently creating long-wavelength streamwise waviness. Despite the presence of such geometrical deviations from an ideal wing and their long known importance to the transition scenario (see e.g. Holmes *et al.* (1985); Nayfeh *et al.* (1988)), stability calculations are often still performed assuming a perfectly smooth surface. Accounting for finer physical details in the stability calculations of boundary layers is crucial for the design of realistic laminar wings that aim to delay the onset of turbulence.

In one of the earliest works concerning the stability of three-dimensional boundary layers over undulated plates, Masad (1996) found a destabilizing effect that was positively correlated with the amplitude of the undulations. Thomas *et al.* (2016) instead found a stabilization of the primary mode for some cases with sinusoidal surface undulations and cites the importance of surface wavelength and phase. The existence of surface undulations is significant to the stability of the flow and can result in both positive (stabilization) and negative (destabilization) effects on the dominant mode. The parameter space is large and requires an efficient (nonlinear) stability calculation framework to be analyzed thoroughly.

The Nonlinear Parabolized Stability Equations (NPSE) are commonly used to calculate the stability of growing boundary layers. Nevertheless, their application is limited due to the assumption of slowly varying perturbation shape. This assumption appears to be valid for smooth surfaces with limited localized surface gradients as shown by Park & Park (2013) and Park & Oh (2020). The PSE have therein been shown to be effective in predicting the stability around localized curvature for 2-dimensional boundary layers. Franco Sumariva *et al.* (2020) show that sharp geometric features break this assumption and require a fully elliptic stability method instead. Additionally, the step size limitation, inherent in the PSE methodology, is mentioned as a crucial limitation for stability over smooth humps. A relaxation of the step size restriction that would allow for finer streamwise discretization is not considered explicitly in that work. Thomas *et al.* (2016) analyzed the linear stability of a swept wing featuring sunsoidal surface deformations with LPSE and Linear Harmonic Navier-Stokes (LHNS), thus establishing some validity of the PSE assumption in undulated surface boundary layer cases, even for cases with small separation regions in the basic state.

Based on the afformentioned studies, the PSE are used for this problem due to the unrivaled speed by which nonlinear simulations can be performed. This allows for a parametric study to be performed that considers also the shape of the undulations. This study aims to analyze the effect of undulation shape on the stability of three-dimensional boundary layers and show the effectiveness of the PSE framework for this type of problem.

Nondimensionalization

In this work, all quantities are presented nondimensionally. Distances are normalized by the boundary layer thick-

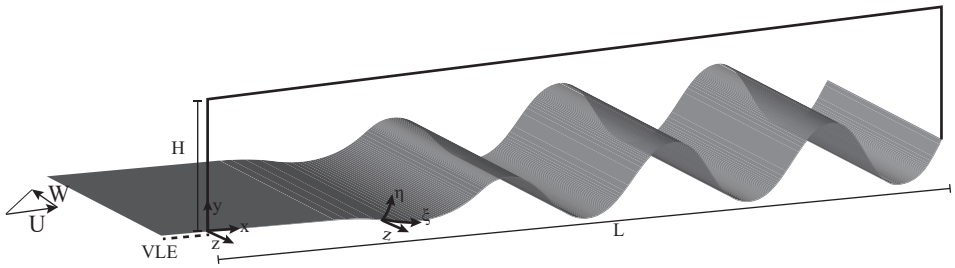

Figure 1. Schematic of a sinusoidally undulated swept plate and the computational domain.

ness, taken as δ_{99} at the inflow, i.e. the reference length denoted $l_{ref} = 7.71 \cdot 10^{-4}$ m. The inflow velocity $U_0 = 15.1$ m/s is used to normalize velocities. A global Reynolds number is defined using these constants and the kinematic viscosity $\nu = 1.51 \cdot 10^{-5}$ m/s^2 as: $Re = \frac{U_0 * l_{ref}}{\nu}$.

Problem Statement

The stability of the boundary layers over swept plates with respect to the freestream flow direction is considered. A schematic of the problem is shown in figure 1. The virtual leading edge is shown upstream of the computational stability domain meaning that a pre-existing boundary layer and crossflow instability is present at the inflow. The computational domain $L = 470 \cdot l_{ref}$ (0.3m). The undulation starts at a distance of $27 \cdot l_{ref}$ (2 cm) downstream of the inflow, ramping up to the maximum amplitude at a distance of 162 l_{ref} (12.5 cm) downstream of the inflow. This is explained in more detail later in this section. The spanwise component of the external flow is constant, $W_\infty = -1.24 \cdot U_\infty$, the streamwise velocity is a function of the leading edge orthogonal dimension, x, following the external velocity distribution of the experiments of Rius-Vidales & Kotsonis (2021) as described in Casacuberta *et al.* (2021).

The transition scenario on swept-wings is generally governed by the evolution of stationary crossflow instabilities due to the low freestream turbulence found in free-flight conditions as noted by Bippes & Müller (1990) and Deyhle & Bippes (1996). In this work, therefore, no travelling crossflow modes are considered and for all modes $\omega = 0$. For the flat plate case, it was found that the mode specified by the spanwise wavelength of $\lambda_z = 7.5$mm is the most unstable mode and thus this mode will be introduced at the inflow for all cases. It is possible that the undulations affect the stability of the boundary layer in such a way that other modes govern the transition scenario instead. A more robust transition analysis would therefore require a nonlinear N-envelope analysis that is considered out of the scope of this work however.

The nonlinear stability of several variations of streamwise surface undulations is considered. After a flat plate region downstream of the inflow, a growing sinusoidal function is altered to either contain a skew or a flat top to assess the effect of the undulations' shape. For the undulations, the shape is described by algebraic functions subject to either the skew parameter $k(=[3,5,7,1000])$, or shape parameter $b(=[0,1,1.5,2])$. These parameters appear in the surface shape functions as:

$$y_w(x) = r(x) \cdot h \cdot \mathtt{Norm}\Big[tan^{-1}\Big(\frac{sin(s)}{k+1-cos(s)}\Big)\Big] \quad (1)$$

$$y_w(x) = r(x) \cdot h \cdot \sqrt{\frac{1+b^2}{1+b^2 \cdot sin^2(s)}} sin(s) \quad (2)$$

Here, Norm indicates a normalization of the shape and $s(x) = \frac{(x-S)2\pi}{\lambda_w}$, where λ_w is the streamwise wavelength of the undulations, S is a constant offset before which the plate is flat, h is the undulation height, and k is a constant skew parameter. The ramp, $r(x) = tanh\Big(20 \cdot l_{ref}(x-S)\Big)$, ensures a smooth introduction of the waviness. Note that the cases described by $k = 1000$ and $b = 0$ are the same case as these shapes approximate a sine function.

The amplitude can be adjusted through the parameter h although it is maintained at $h = 0.3059 \cdot l_{ref}$ in this work. Still, it will be shown that this small undulation amplitude has a noticeable effect on the stability of the base flow. The base flow does not feature any separation for the cases presented here. The geometric shape of the undulation can be adjusted to be more square by varying the parameter b in equation 2. The resulting surfaces are shown below in figure 2.

Methodology

The stability of swept undulated plates is considered nonlinearly using the NPSE methodology. The NPSE are derived for generalized coordinates, parabolizing the equations in the body-fitted grid along the streamwise direction. The basic state is found using the steady incompressible laminar Navier Stokes formulation in the commercial finite element solver COMSOL. The details for both the base flow solver and PSE methods are presented in this section.

In COMSOL, the inflow is prescribed by an analytical Falkner-Scan-Cooke solution. At the wall, the no-slip condition is imposed and a pressure description of a favourable pressure gradient is prescribed at the top boundary as found in Casacuberta *et al.* (2021). This top boundary is placed at a height, H, which through preliminary investigations is found to have no influence on the results ($H = 51.9 * l_{ref}$). The outlet prescribes a constant static pressure condition equal to the static pressure found at the top boundary at that streamwise location. Two finite elements are present in the spanwise direction, z, with periodic boundary conditions. Velocities and

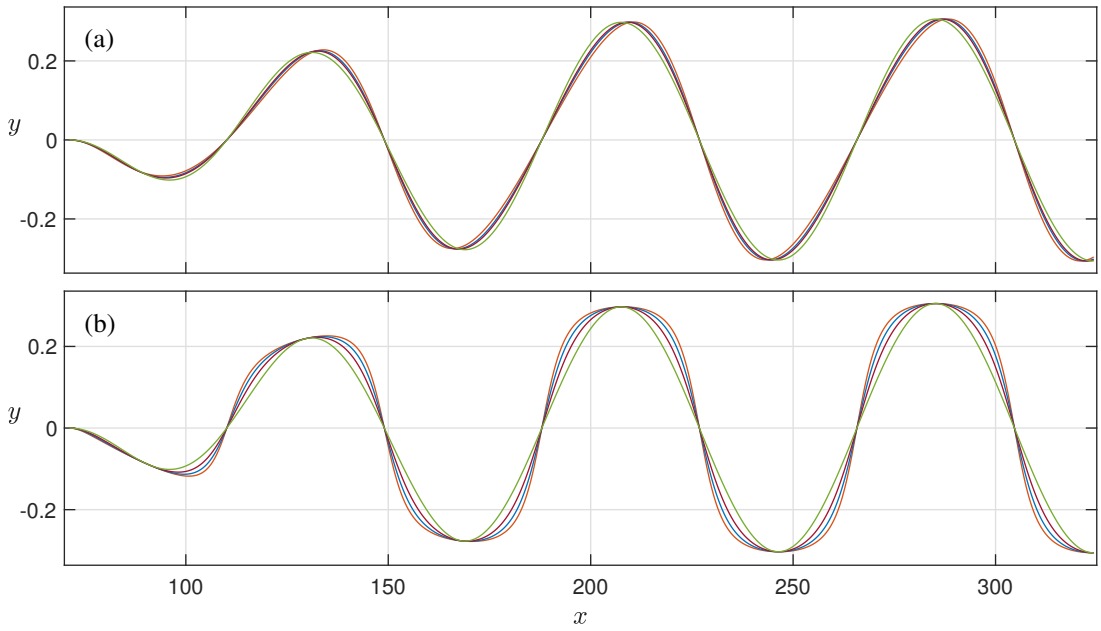

Figure 2. Surface undulations (not to scale) for the (a) skewed sinusoidals with k =[1000 7 5 3] and (b) squared sinusoidals with b =[2.5 2 1.5 0] in orange, blue, purple and green respectively.

pressures are calculated using second-order elements of which there exist 78 in the wall-normal direction clustered to the wall and 877 equispaced in the streamwise direction, using a direct solver procedure.

To analyze the stability of the basic state, a body-fitted coordinate system is introduced with the ξ-axis at $\eta = 0$ being locally parallel and normal to the wall surface. The η-coordinate is constructed such that the grid is locally orthogonal at the wall as is required for parabolization along the ξ-axis. After a perturbation analysis is performed on the generalized Navier-Stokes equations, the nonlinear solution ansatz is introduced:

$$q'(\xi,\eta,z,t) = \sum_m \sum_n \hat{q}_{m,n}(\xi,\eta) e^{\mathrm{i}\left(\int_{\xi_s}^{\xi_e} \alpha(\xi) d\xi^* + \beta_n z - \omega_m t\right)} + \text{c.c} \tag{3}$$

Here q' is the perturbation state vector $[u', v', w', p']^T$ described by a truncated sum of modes denoted by m and n for angular frequency ω, and spanwise wavelength, β, respectively. The streamwise wavenumber, α, is complex with the real part describing the wavenumber and the imaginary part the growth rate. The * denotes an integration variable. Lastly, t is the time, i is the imaginary unit and c.c denotes the complex conjugate.

The resulting equations, in generalized coordinates, are presented in system form as:

$$\mathbb{L}\hat{q} + \mathbb{M}\frac{\partial \hat{q}}{\partial \xi} + \mathbb{N}\frac{\partial \alpha}{\partial \xi}\hat{q} = r \tag{4}$$

Where $\mathbb{L}$, $\mathbb{M}$ and $\mathbb{N}$ are:

$$\mathbb{L} = \begin{bmatrix} L + \frac{\partial U}{\partial x} & \frac{\partial U}{\partial y} & 0 & i\alpha\xi_x + \eta_x D_1 \\ \frac{\partial V}{\partial x} & L + \frac{\partial V}{\partial y} & 0 & \eta_y D_1 + i\alpha\xi_y \\ \frac{\partial W}{\partial x} & \frac{\partial W}{\partial y} & L & i\beta \\ i\alpha\xi_x + \eta_x D_1 & i\alpha\xi_y + \eta_y D_1 & i\beta & 0 \end{bmatrix}$$

$$\mathbb{M} = \begin{bmatrix} M & 0 & 0 & \xi_x \\ 0 & M & 0 & \xi_y \\ 0 & 0 & M & 0 \\ \xi_x & \xi_y & 0 & 0 \end{bmatrix}$$

$$\mathbb{N} = \begin{bmatrix} -\frac{i}{Re}(\xi_x^2 + \xi_y^2) & 0 & 0 & 0 \\ 0 & -\frac{i}{Re}(\xi_x^2 + \xi_y^2) & 0 & 0 \\ 0 & 0 & -\frac{i}{Re}(\xi_x^2 + \xi_y^2) & 0 \\ 0 & 0 & 0 & 0 \end{bmatrix}$$

$$r = \begin{bmatrix} -u\frac{\partial u}{\partial \xi}\xi_x - u\frac{\partial u}{\partial \eta}\eta_x - v\frac{\partial u}{\partial \xi}\xi_y - v\frac{\partial u}{\partial \eta}\eta_y - i\beta \mathbf{u}w \\ -u\frac{\partial v}{\partial \xi}\xi_x - u\frac{\partial v}{\partial \eta}\eta_x - v\frac{\partial v}{\partial \xi}\xi_y - v\frac{\partial v}{\partial \eta}\eta_y - i\beta \mathbf{v}\mathbf{w} \\ -u\frac{\partial w}{\partial \xi}\xi_x - u\frac{\partial w}{\partial \eta}\eta_x - v\frac{\partial w}{\partial \xi}\xi_y - v\frac{\partial w}{\partial \eta}\eta_y - i\beta \mathbf{w}^2 \\ 0 \end{bmatrix},$$

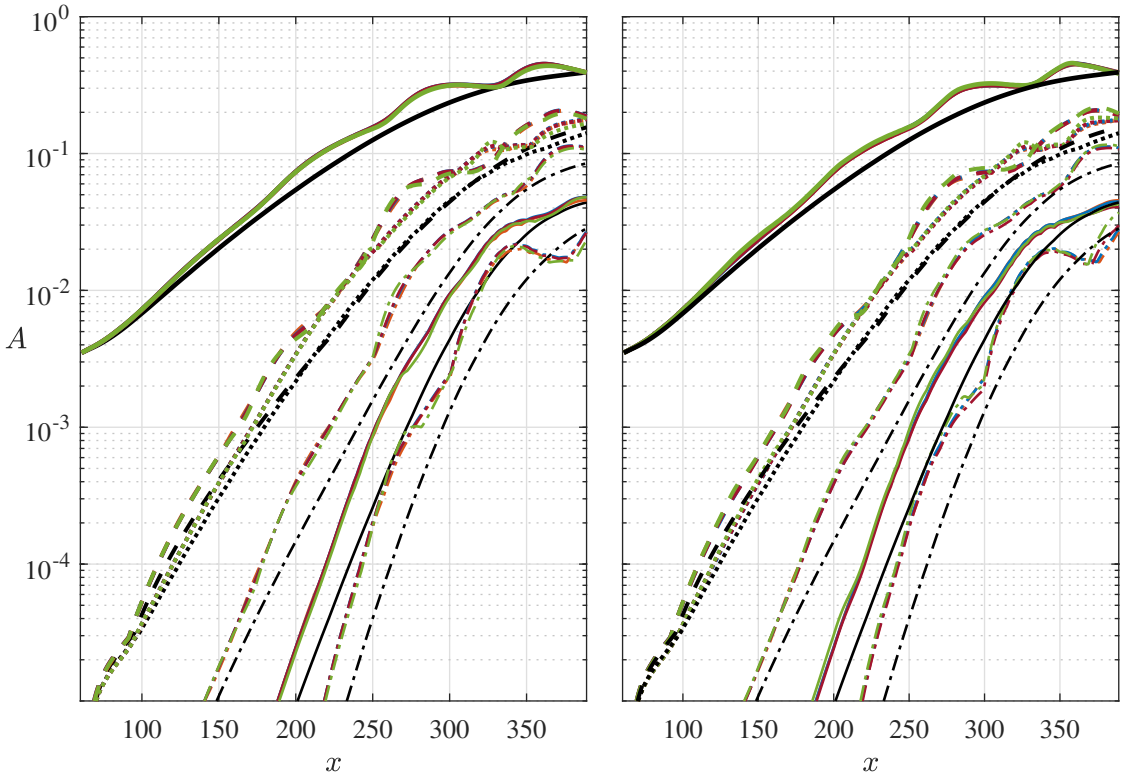

Figure 3. Amplitude evolution of the 1st (thick line), 2nd (dashed), 3rd (dash-dotted), 4th (thin line) and 5th (thin dash-dotted) harmonic and the mean flow distortion (dotted) over swept plates with (a) skewed surface undulations k =[1000 7 5 3] and (b) square sinusoidals with b =[0 1 1.5 2] in orange, blue, red and green respectively. The reference CFI evolution over a flat plate is shown in black.

With D_1 and D_2 derivative matrices and

$$L = -i\omega + iU\alpha\xi_x + U\eta_x D_1 + i\alpha V\xi_y + V\eta_y D_1 + i\beta W + \frac{1}{Re}(\alpha^2(\xi_x^2+\xi_y^2)+\beta^2) - \frac{1}{Re}(\eta_x^2+\eta_y^2)D_2 - \frac{1}{Re}2i\alpha(\eta_y\xi_y+\eta_x\xi_x)D_1 - \frac{1}{Re}i\alpha(\xi_{yy}+\xi_{xx}) - \frac{1}{Re}(\eta_{xx}+\eta_{yy})D_1 \tag{5a}$$

and

$$M = U\xi_x + V\xi_y - \frac{2i\alpha}{Re}(\xi_x^2+\xi_y^2) - (\xi_{xx}+\xi_{yy})\frac{1}{Re} - \frac{2(\eta_y\xi_y+\eta_x\xi_x)}{Re}D_1 \tag{6a}$$

It must be noted that the base flow derivatives are still present in these equations as derivatives with respect to the physical xy-coordinate system as they are constants to the stability problem. Furthermore, the last column of $\mathbb{M}$ can be neglected, effectively multiplying the streamwise pressure derivative $\frac{\partial p}{\partial \xi}$ by 0 for all modes as suggested by Li & Malik (1996), in order to relax the step size restriction of the NPSE. Although this step can be performed reliably in most flat plate stability simulations, more complex geometries require a careful consideration as the streamwise pressure gradient of the perturbations might not be negligible. To ensure this step is valid, a linear validation was also performed neglecting the $\frac{\partial p}{\partial \xi}$, as will be shown in the following section.

Guaranteeing the numerical stability of the NPSE is difficult for the discussed cases, though it can be improved in several ways if a fine enough base flow simulation is used. In the present work, some additional measures are taken to this goal, by adding the mean flow distortion to the base flow after a transformation of the derivatives to the physical coordinate frame. This effectively reduces the weight of the right-hand side, as the effect of the mean flow distortion is accounted for in the left-hand side rather than through modal interactions as was suggested by Zhao *et al.* (2016). Additionally, the nonlinear forcing term is subjected to an under-relaxation factor of 0.2 in the nonlinear convergence iteration. Lastly, the convergence procedure is split in two steps as shown by Park & Park (2011), specifically: First, for a given forcing term, the α is converged for all modes. Then, the forcing term is updated and the process is repeated until, again, the streamwise wavenumber is converged.

The NPSE are discretized in 400 stages in the streamwise direction ($\Delta\xi = 0.88$) using a first-order backward implicit Euler scheme. In the wall-normal direction spectral colocation is employed incorporating 80 Chebyshev polynomials on an equal number of collocation points that are clustered near the wall. The initial condition for the primary mode is created by solving the local eigenvalue problem for the perturbation velocities, pressure and the complex-valued streamwise wavenumber. The desired nondimensional initial amplitude, $A_0 = 1.75 \cdot 10^{-3}$ based on the maximum of the streamwise perturbation velocity, is then imposed on the primary mode

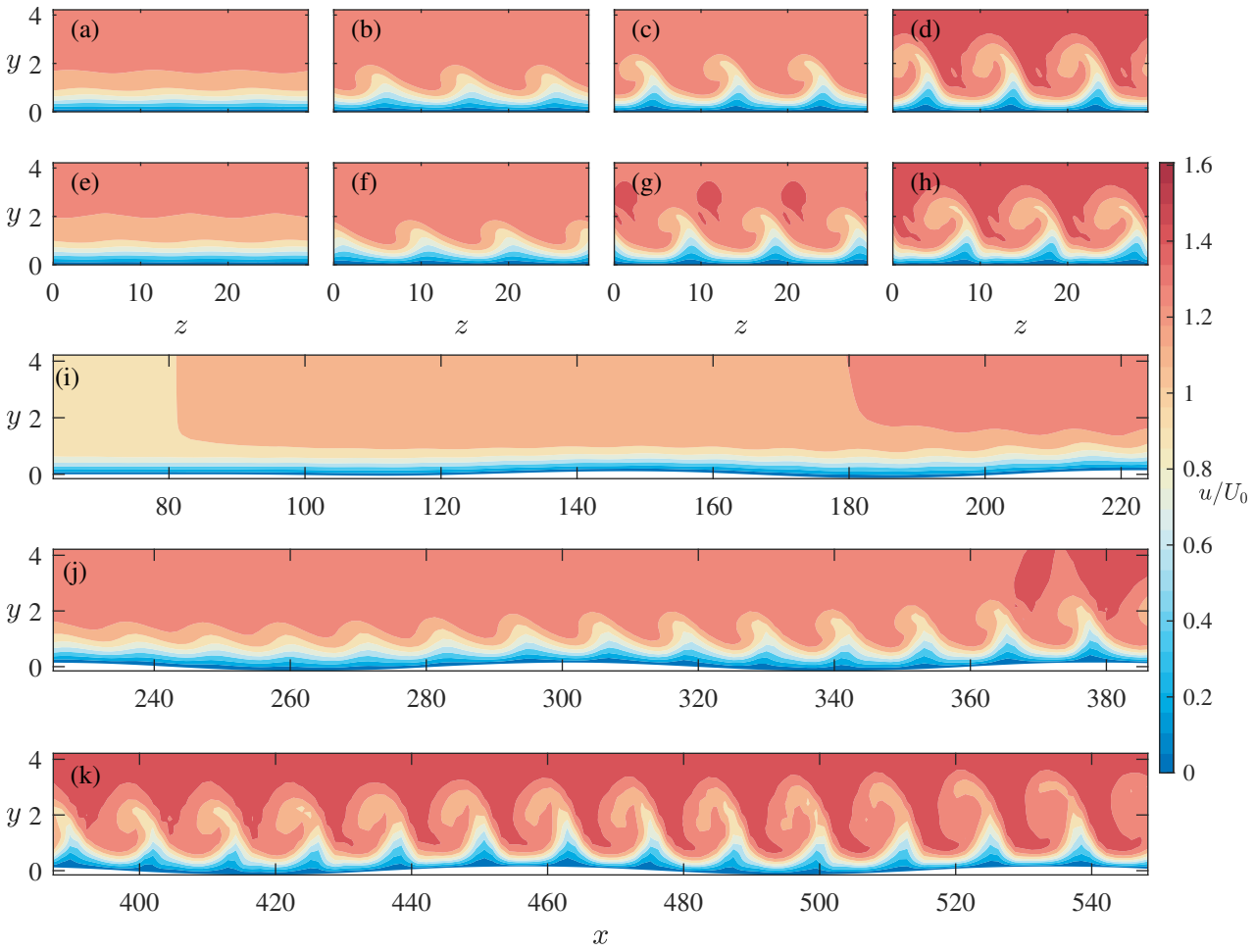

Figure 4. Fully reconstructed velocity fields based on the sum of base flow and instability modes. Streamwise velocity in the yz-plane for the flat plate case (a-d) and the undulated plate (e-h) with k = 1000 at x = 182 (a,e), x = 305 (b,f), x = 367(c,g) and x =427 (d,h) with the $y = 0$ representing the local wall location. Contours of streamwise velocity in the xy-plane over the entire streamwise domain (i,j,k).

and its complex conjugate. The nonlinear terms are incorporated explicitly in the equations through a forcing term on the right-hand side. For all stability simulations, five harmonics and the mean flow distortion are considered while higher harmonics are suppressed even if they are predicted to cross the nonlinear introduction threshold of $A = 1 \cdot 10^{-08}$.

The base flows capture all features and the base flow profiles and derivatives were ensured to be smooth throughout the domain, however, the base flow was not subjected to a systematic grid convergence study and it is hypothesized that the numerical stability and convergence of the NPSE can be significantly improved through the use of finer base flows.

Validation of the PSE Assumption in mildly undulating flows

The PSE assumption of slowly varying flow is validated for the primary mode by comparing the linear PSE result with results from a harmonic Navier-Stokes (HNS) simulation that does not neglect higher-order derivatives. This validation is assumed to be independent of the harmonic considered as it applies to the shape function, rather than the total mode. Therefore, a linear match between the two methods would point toward the validity of the slowly varying flow assumption for both the linear and nonlinear system.

Figure 5 shows a comparison between the linear amplitude evolution as calculated per PSE and HNS for the case with the strongest wall gradients ($b = 1.5$), proving the validity of neglecting the higher order derivatives in the PSE derivation.

Results

Base flow simulations were performed for all undulated plates of section and the reference swept flat plate case. The basic states were then used to perform nonlinear stability calculations using the NPSE. The base flows show no flow separation due to the mild amplitude of the waviness.

The amplitude evolution is shown separately for the skewed sinusoidal and squared sinusoidal cases in figure 3(a) and (b) respectively. In all reported cases, the growth of the crossflow instability is enhanced by the surface undulations. The local effect of the surface undulations is clearly visible for all cases, although the differences between the cases are minor indicating that the shape is not critically important to the stability response of the boundary layer within the investigated parameter space.

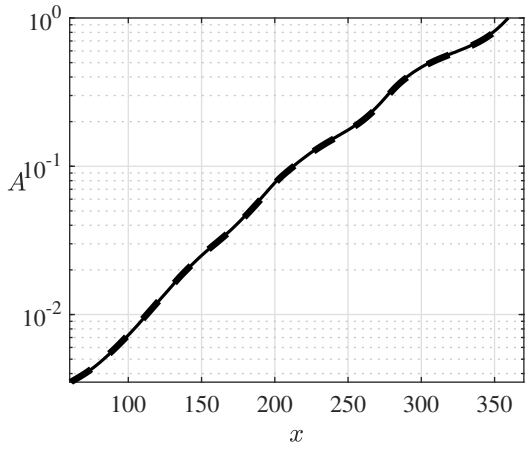

Figure 5. Linear amplitude evolution of the primary crossflow instability mode ($\lambda_z = 9.7 \cdot l_{ref}$, $\omega = 0$) as calculated per PSE (line) and HLNS (dashed) for the case $b = 1.5$.

It should be noted that the validity of NPSE, judged here by the ability of the NPSE to converge in the presented domain and providing a linear match with HNS results, is limited and depends strongly on the geometry (shape and amplitude) of the wall. For the current case, a greater undulation amplitude ($h > 0.3059 \cdot l_{ref}$), stronger skew ($k < 3$) or more square shape ($b > 3$) could affect the accuracy of the results.

In figure 4, streamwise velocity contours taken from the fully reconstructed flowfield are depicted. In figures 4(a-d) the evolution over a flat plate is shown, which can be directly compared to the results of 4(e-h) below, showing the contours at the same streamwise location for the sinusoidal plate. The comparison highlights the deformation of the developed crossflow instability in the strongly nonlinear regime for the undulated plate. In figures 4(i-j) xy-planes of the streamwise velocity contours are shown demonstrating the relative scale of the surface undulations compared to the incoming perturbation. The streamwise wavelength of the undulation is approximately six times that of the perturbation and the height is a just under half the vortex core height. The effect of the mild undulations is visible in the contours of the crossflow vortex which is in accordance with the discovered effect on the amplitude evolution.

Conclusion

The effect of surface undulations on the nonlinear evolution of crossflow instabilities was considered for several wall surface undulation shapes.

The local effect of the wall shape variations was found to be strong and can be directly explained by considering the effect on the pressure gradient and curvature. Any undulation considered in this work strongly affects the local stability of the primary mode directly. Across all undulation shapes a rising wall expectedly promotes the growth of the incoming CFI as a result of the pressure gradient becoming more favourable. After the apex, the pressure gradient becomes more adverse and the growth of crossflow instabilities is instead reduced.

The behaviour of higher harmonics is found to be more affected by the nonlinear forcing, governed by the primary mode, than by the linear effect of the wall shape present in the base flow and curvature terms.

As mentioned in the introduction, the parameter space for wall-undulations is too large to cover in this work. The effects of wavelength, phase, shape and amplitude need to be considered. This work could only tackle the effect of undulation shape limited by the PSE assumptions. All cases caused an accumulated destabilization of the crossflow instabilities which could lead to a significant advancement of the transition front. Consequently, it is concluded that surface undulations have to be accounted for in stability analysis if present at amplitudes of a similar scale as presented here.

REFERENCES

Bippes, H & Müller, B 1990 Disturbance growth in an unstable three-dimensional boundary layer. In *Numerical and Physical Aspects of Aerodynamic Flows IV*, pp. 345–358. Springer.

Casacuberta, Jordi, Hickel, Stefan & Kotsonis, Marios 2021 Mechanisms of interaction between stationary crossflow instabilities and forward-facing steps. In *AIAA Scitech 2021 Forum*, p. 0854.

Deyhle, H & Bippes, H 1996 Disturbance growth in an unstable three-dimensional boundary layer and its dependence on environmental conditions. *Journal of Fluid Mechanics* **316**, 73–113.

Franco Sumariva, Juan Alberto, Hein, Stefan & Valero, Eusebio 2020 On the influence of two-dimensional hump roughness on laminar–turbulent transition. *Physics of Fluids* **32** (3), 034102.

Holmes, Bruce J, Obara, Clifford J, Martin, Glenn L & Domack, Christopher S 1985 Manufacturing tolerances for natural laminar flow airframe surfaces. *SAE Transactions* pp. 522–531.

Li, Fei & Malik, Mujeeb R 1996 On the nature of pse approximation. *Theoretical and Computational Fluid Dynamics* **8** (4), 253–273.

Masad, Jamal A 1996 Effect of surface waviness on transition in three-dimensional boundary-layer flow. *Tech. Rep.*.

Nayfeh, Ali H, Ragab, Saad A & Al-Maaitah, Ayman A 1988 Effect of bulges on the stability of boundary layers. *The Physics of fluids* **31** (4), 796–806.

Park, Donghun & Oh, Sejong 2020 Effect of shape of two-dimensional smooth hump on boundary layer instability. *International Journal of Aeronautical and Space Sciences* **21** (4), 906–923.

Park, Donghun & Park, Seung O 2013 Linear and non-linear stability analysis of incompressible boundary layer over a two-dimensional hump. *Computers & Fluids* **73**, 80–96.

Park, Dong-Hun & Park, Seung-O 2011 Nonlinear stability analysis of boundary layers by using nonlinear parabolized stabiltiy equations. *Journal of the Korean Society for Aeronautical & Space Sciences* **39** (9), 805–815.

Rius-Vidales, Alberto F & Kotsonis, M 2021 Impact of a forward-facing step on the development of crossflow instability. *Journal of Fluid Mechanics* **924**.

Thomas, Christian, Mughal, Shahid M, Gipon, Matthew, Ashworth, Richard & Martinez-Cava, Alejandro 2016 Stability of an infinite swept wing boundary layer with surface waviness. *AIAA Journal* **54** (10), 3024–3038.

Zhao, Lei, Zhang, Cun-bo, Liu, Jian-xin & Luo, Ji-sheng 2016 Improved algorithm for solving nonlinear parabolized stability equations. *Chinese Physics B* **25** (8), 084701.